Dividing the spoils: The role of pyrazine ligands and perchlorate counterions in the magnetic properties of bis(pyrazine)diperchloratecopper(II), [Cu(pz)$_2$](ClO$_4$)$_2$, compound

Sergi Vela[1], Joaquim Jornet-Somoza[1,2], Mark M. Turnbull[3], Ralf Feyerherm[4], Juan J. Novoa[1], Mercè Deumal[1,*]

[1] Departament de Química Física & IQTCUB, Facultat de Química, Universitat de Barcelona, Martí i Franquès 1, 08028-Barcelona, Spain
[2] Institut Charles GERHARDT-CNRS 5253, Université Montpellier 2, CC15001, Place Eugène Bataillon, 34095 Montpellier, France
[3] Carlson School of Chemistry and Biochemistry, Clark University, 950 Main St. Worcester, MA 01610, USA
[4] Helmholtz-Zentrum Berlin für Materialien und Energie, 14109 Berlin, Germany

email: merce.deumal@ub.edu

ABSTRACT

A complete First-Principles Bottom-Up computational study of the magnetic properties of [Cu(pz)$_2$](ClO$_4$)$_2$ is presented. A remarkable agreement is observed in the whole range of temperatures between simulated and experimental magnetic susceptibility data. Interestingly, the simulated heat capacity values show an anomaly close to the Néel temperature of 4.21 K associated with a transition from a 2D antiferromagnet to a 3D ordered state. The antiferromagnetic behavior of [Cu(pz)$_2$](ClO$_4$)$_2$ is due to a 2D magnetic topology owing to two antiferromagnetic J_{AB} interactions through pyrazine ligands. Although presenting a very similar molecular arrangement, the numerical values of the two magnetically significant J_{AB} couplings differ by 25% (-10.2 vs. -7.3 cm^{-1}). This difference is found it can be ascribed to three main contributions: (i) the central pyrazine ring *shearing*-like distorsion, (ii) the effect of the orientation of the perchlorate counterions, and (iii) a hitherto skeleton-counterion cooperation arising from different hydrogen bonding contribution in the two most significant J_{AB} couplings. The impact of the orientation of the perchlorate counterions is disclosed by comparison to J_{AB} studies using structurally similar ligands but with different electronegativity (namely BF$_4^-$, BCl$_4^-$, and BBr$_4^-$). Pyrazine ligands and perchlorate counterions prove to be non-innocent .

INTRODUCTION

Much work has been devoted for decades to the design and synthesis of materials with low magnetic dimensionality, especially since the discovery that copper-based high T_c superconductors are well-isolated 2D-Heisenberg antiferromagnets (AFM). Within the framework of 2D AFM, previous studies upon copper pyrazine compounds have revealed their ability to form chains[1] and layered structures.[2] Therefore, copper pyrazine based complexes have become excellent candidates to obtain 2D AFM topologies.

Several mathematical models[3] have been used extensively to fit the available experimental magnetic data (e.g. magnetic susceptibility $\chi(T)$), and ultimately predict the magnetic topology of these materials. However, the lack of proper analytical fitting expressions to describe some 2D topologies and the fact that different models can produce similarly-shaped $\chi(T)$ curves make it necessary to resort to other methodologies.[4] Among them, we would like to highlight the exhaustive evaluation of the magnetic properties through theoretical simulations, without *a priori* magnetic topology assumptions. Specifically, our research is conducted according to a First-Principles Bottom-Up approach,[5] which has been demonstrated to be reliable at interpreting and rationalizing the magnetic properties of both organic and metal-based molecular magnetic systems. [6, 7, 8, 9]

We have shown that theoretical studies can help in interpreting the magnetism in several copper-based prototype complexes with magnetic topologies ranging from spin-ladders to 3D magnets.[6] In fact, recently, two copper pyrazine antiferromagnets have been the subject of our research, namely, (pyrazine)dinitratocopper(II),[7] $Cu(pz)(NO_3)_2$, and bis(2,3-dimethyl pyrazine)dihalocopper(II),[8] $Cu(2,3-dmpz)_2X_2$ where X=Cl, Br. Note that in both molecule-based magnets all ligands and counterions are closed-shell species. The first system was supposed to be a prototype of 1D isolated AFM chains until it was discovered that it underwent transition to 3D long-range order at 0.107K, facts that were theoretically rationalized.[7] The latter was found to be a strong-rung (through halide) ladder, and a comparative study was performed to unravel why $J(Cu \cdots X_2 \cdots Cu)$ magnetic exchange was similar irrespective of X being Cl or Br, unlike $J(Cu \cdots pz \cdots Cu)$ which was halogen dependent.[8] After studying these two low-dimensional AFMs theoretically, the logical step ahead is thus to choose a potential 2D Heisenberg AFM. As stated in the literature,[10] bis(pyrazine) diperchloratocopper(II) $[Cu(pz)_2](ClO_4)_2$ (**1**)[2d] is a good candidate to explore lattice and

exchange anisotropies as well as field-induced anisotropy. Besides, muon spin-relaxation ($\mu-SR^+$) measurements have revealed that $[Cu(pz)_2](ClO_4)_2$ undergoes a transition from a 2D antiferromagnet to a 3D ordered state at 4.21 K.[11] Therefore, $[Cu(pz)_2](ClO_4)_2$ (**1**)[2d] has been selected as a new challenge not only for an in-depth First-Principles Bottom-Up study of its experimental magnetic properties (magnetic susceptibility and heat capacity) but also for exploring the origin of the 2D AFM to 3D ordered state transition.

$[Cu(pz)_2](ClO_4)_2$ radicals are formed by copper (II) cations coordinated to four pyrazine (pz) molecules and two perchlorate anions, which are arranged in a tetragonally elongated octahedron coordination[2d,12] (see Figure 1a; note that the perchlorate anions lie on the elongated Jahn-Teller axis). Each pyrazine molecule bridges two Cu(II) ions. Experimentally, perchlorate ions, ClO_4^-, are supposed to be non-coordinating or poorly coordinating anions.[2d] The $[Cu(pz)_2](ClO_4)_2$ unit has a doublet ground state due to the fact that copper (II) has one unpaired electron while pyrazine and perchlorate are closed-shell species. In order to confirm the 2D magnetic topology proposed experimentally for this system, a First-Principles Bottom-Up study of **1** is carried out to evaluate the J_{AB} magnetic couplings present in the crystal and reproduce the experimental magnetic data. In addition, the role of the pyrazine ligands and perchlorate counterions is fully addressed. The study is done for two crystal structures of the same polymorph at two temperatures (10K and 163K) in order to also test the impact of thermal expansion on the magnetic properties of this crystal.
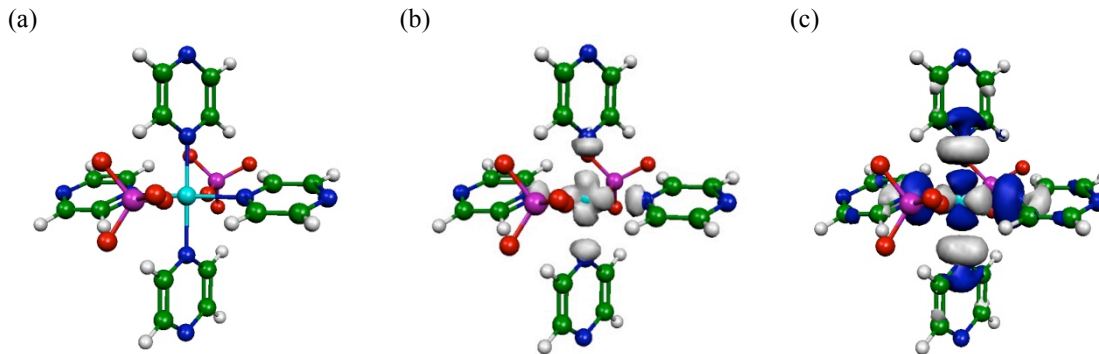

Figure 1: (a) Geometry and (b) spin density of $[Cu(pz)_2](ClO_4)_2$ radical (color code: Cu=light blue, Cl=purple, O=red, N=blue, C=green, H=grey). (c) Representation of the radical SOMO at 0.02 a.u. cutoff value.

Table 1. Crystal data and structure refinement for deuterated **1** at 10 K and 163 K, which are denoted as **1-10K** and **1-163K**, respectively.

	1-10K	**1-163K**[2d]
Empirical formula:	$C_8D_8N_4O_8Cl_2Cu$	$C_8D_8N_4O_8Cl_2Cu$
Formula weight	430.67	430.67
Radiation	Neutron 1.79803(2) Å	X-Ray, $\lambda = 0.71073$
Crystal system	Monoclinic	Monoclinic
Crystal habit	Blue powder	Blue plate
Space group	*C2/c*	*C2/c*
Unit cell dimensions:		
a (Å)	13.8147(48)	14.072(5)
b (Å)	9.7108(33)	9.786(3)
c (Å)	9.7686(33)	9.781(3)
β (°)	97.3488(40)	96.458(4)
Z	4	4
Size(mm)	powder	0.4 x 0.2 x 0.02
Data collection:		
Temperature (K)	10(1)	163(2)
Reflections collected	817	8026 (1379 unique)
θ range (°)	4 – 70	2.55 – 26.52
Range h, k, l	$0 \leq h \leq 14$	$-17 \leq h \leq 17$
	$0 \leq k \leq 10$	$-11 \leq k \leq 12$
	$0 \leq l \leq 10$	$-12 \leq l \leq 11$
Refinement:		
Data/rest./para.	817/0/71	1379/0/85
Rietveld R-factors		$R_1 = 0.0351$ (I>2σ)
R_p	4.23 %	$R_1 = 0.0347$ (all data)
R_{wp}	5.58 %	
R_{exp}	1.28 %	

EXPERIMENTAL DETAILS

1. Synthesis:

Cu(d$_4$-pyrazine)$_2$(ClO$_4$)$_2$ was synthesized, according to the published procedure,[2d] by dissolving d$_4$-pyrazine and Cu(ClO$_4$)$_2$ hexahydrate in a 2:1 ratio in D$_2$O and placing the resulting solution in a desiccator. Over the course of a week, the blue crystalline product, Cu(d$_4$-pyrazine)$_2$(ClO$_4$)$_2$, appeared. It was isolated by vacuum filtration, washed with cold D$_2$O and allowed to air dry, giving 74% yield. Powder X-ray diffraction verified that the deuterated material was isomorphous with the protonated material. Based upon refinement, the material was ~95% deuterated.

2. Neutron Diffraction Data Collection:

Neutron diffraction at 10 K was carried out at the BER-II reactor of the Helmholtz-Zentrum Berlin using the fine-resolution powder diffractometer E9. The neutron wavelength provided by the Ge monochromator was 1.7980 Å. The sample was encapsulated in a vanadium can and cooled in a ^{4}He-flow cryostat. Rietveld analysis of the diffraction data was carried out using the WinPLOTR/Fullprof package.[13] The diffraction data showed that the sample was a single phase. The refinement indicated a degree of deuteration of 93%. The structural parameters observed at 10 K, relevant for the present study, are listed in Table 1. The cif file is available free of charge at http://www.ccdc.cam.ac.uk/products/csd/request/request.php4 (CCDC-896598). The 163 K crystal structure of **1** (CCDC-203407) was reported previously.[2d]

COMPUTATIONAL DETAILS

The First-Principles Bottom-Up work strategy[5] allows the computation of the macroscopic magnetic properties of a molecule-based crystalline material from only the knowledge of the experimental crystal structure. No assumptions are made concerning the sign or size of the radical pair magnetic interactions within the crystal. It is a four-step procedure described as follows.

One must first analyze the crystal packing in order to identify all unique radical···radical pairs that are likely to be magnetically active, irrespective of being through-bond or through-space magnetic interactions. Then, in a second step, one must proceed to calculate the radical···radical magnetic interactions (J_{AB}) for all unique pairs previously identified. The J_{AB} interactions in crystals of **1** formally originate in the Cu(II) ions. However, although Cu(II) ions formally hold one unpaired electron, calculation of the spin density carried out for the $[Cu(pz)_4](ClO_4)_2$ radical shows that the spin density spreads over the adjacent pyrazine rings (mostly on its nitrogen atoms) as well as over the Cu(II) ion (see Figure 1b). This is also true for the SOMO, which delocalizes mainly over the nitrogen atoms of the adjacent pyrazine rings (note the antibonding nature of the SOMO of $d_{x^2-y^2}$ character in Figure 1c and Supporting Information S1). In order to reproduce properly the electronic structure of the interacting electrons, each Cu(II) radical is coordinated to four pyrazine ligands and two ClO_4^- counterions at their crystal geometry. The resulting $[Cu(II)(pz)_4](ClO_4)_2$ radical unit is a doublet and has zero net charge. Since the Heisenberg Hamiltonian used for the calculation of

J_{AB} exchange couplings is the isotropic Hamiltonian $\hat{H} = -2\sum J_{AB}\hat{S}_A \cdot \hat{S}_B$ (1), the exchange anisotropy (XY vs. Heisenberg) will not be evaluated. According to the Hamiltonian (1), the value of J_{AB} for each AB pair is computed as the energy difference between the open-shell singlet S and triplet T states, $\Delta E^{S-T} = E^S - E^T = 2J_{AB}$. The Broken Symmetry, *BS*, approach[14] was used to properly describe the open-shell singlet state. Since the overlap between magnetic orbitals is small, $\Delta E^{S-T} = 2(E^{BS} - E^T) = 2J_{AB}$.[15] All energy evaluations were performed using the B3LYP functional.[16,17] All SCF energy convergences have been set up at 10^{-7} au., allowing an accuracy of 0.04 cm^{-1} in the evaluation of the magnetic exchange J_{AB} values within the UB3LYP framework. The effect of the basis set is discussed in the Supporting Information, section S2. In view of the results analyzed therein, a TZVP basis set[18] was selected. Atomic charges, when required, were computed according to the Merz-Singh-Kollman (MSK) scheme.[19] All calculations were performed using the Gaussian09[20] package.

Previous experience[21] prompted us to employ a crystal structure determined at the lowest possible temperature, thus minimizing possible anisotropic thermal effects of the crystal packing in the computed J_{AB}. In order to test the relevance of thermal anisotropic effects for [Cu(pz)$_2$](ClO$_4$)$_2$ **1**, the First-Principles Bottom-Up procedure has been applied to the already published 163 K[2d] and to the newly reported 10K crystal structures (referred to as **1-10K** and **1-163K**, respectively, throughout the paper), since those are the only available crystal structures.

In the third step, the magnetic topology is straightforwardly defined by the network of non-negligible J_{AB} interactions. The lattice anisotropy, i.e. magnetic dimensionality, is thus addressed. Then, upon analysis of the magnetic topology, the minimal magnetic model can be chosen. This model should include all significant J_{AB} magnetic interactions in a ratio as close as possible to that found in the infinite crystal, and whose propagation along the crystallographic axes reproduces the magnetic topology of the infinite crystal.

Finally, in the fourth and last step, the computation of the macroscopic magnetic properties (magnetic susceptibility, heat capacity, magnetization, etc.) is performed using statistical mechanics expressions.[22] Based on a regionally reduced density matrix approach,[5] the matrix representation of the Heisenberg Hamiltonian is built and fully diagonalized using the space of spin functions of the selected minimal magnetic model as a basis set. The resulting energy and spin multiplicity of all possible magnetic states are then used in the appropriate statistical mechanics expression[22] to obtain the macroscopic magnetic properties

of **1,** in this instance $\chi(T)$ and $C_p(T)$. In our derivation of $\chi(T)$, for simplicity the magnetic field is taken to be parallel to the easy axis of alignment (if any) ($g\mu_B H \hat{S}_z$). Accordingly, it allows us to compute the magnetic susceptibility parallel to the easy axis ($\chi_\parallel$; hereafter $\chi(T)$). In the case of $[Cu(II)(pz)_4](ClO_4)_2$, a *g*-factor of 2.07 (derived from the fitting of the experimental parallel magnetic susceptibility data)[10] was used for the simulation of the magnetic susceptibility as a function of temperature (see Supporting Information S3 for discussion on magnetic susceptibility data from powder or single crystal samples). Let us remark that contrary to other approaches, our First-Principles Bottom-Up work strategy does not use periodic boundary conditions but a regionally reduced density matrix approach, which in turn is inspired by the real-space renormalization group RSRG with effective interactions approach.[23] Therefore, within the framework of effective Hamiltonian theory, instead of working with the Hamiltonian of the infinite crystal space, we use its projection onto a subspace of the magnetic topology.

RESULTS and DISCUSSION

*1. First-Principles Bottom-Up analysis of the magnetism of [Cu(pz)₂](ClO₄)₂ (**1**).*

The analysis of the 10K-crystal structure of **1** yielded seven unique radical dimers within a Cu···Cu cut-off distance of 10Å, ranging from 6.876Å to 9.769Å and including intra- and inter-layer pairs (see Table 2 and Supporting Information S4). Note that, for a given radical, the radical pairs include all its nearest- and next-nearest neighbors. After computation of open-shell singlet and triplet energies, only four non-negligible[24] *J(di)* values were found (Table 2). Dimers *d1* and *d2* are responsible for most of the magnetic exchange with J_{AB} values of −10.2 cm^{-1} and −7.3 cm^{-1}, respectively. These dimers correspond to pairs of radicals that are connected through a pyrazine ring (Figure 2a-b) and arranged to form isolated magnetic *bc*-layers. In contrast, dimers *d3* and *d4*, with almost negligible J_{AB} values (−0.3 cm^{-1}), correspond to neighboring radicals that are not connected through a pyrazine ring but through-space at a rather long Cu···Cu distance (> 9.7 Å). Interlayer dimers *d5*, *d6* and *d7* have no significant magnetic interactions despite being in the range of 7.9 to 9.0 Å, i.e. at a closer Cu···Cu distance than *d3* and *d4*, indicating that the Cu···Cu distance by itself is not a good indicator of the potential J_{AB} values between radicals. Instead, the magnetic topology is driven by the presence of pyrazine-mediated through-bond magnetic pathways for the dominant

magnetic interactions. Figure 2b shows the 2D magnetic building block of **1**. The absence of significant magnetic interactions for these *d5*, *d6* and *d7* dimers is responsible for the 2D magnetic topology of **1**. The lattice anisotropy is thus responsible for **1** being topologically a 2D magnetic system with each Cu having two neighbors of type-1 (J_1) and two neighbors of type-2 (J_2) (see red and blue lines in Figure 2c, respectively). This is in agreement with the experimentally suggested magnetic pattern.[2d, 11]

Table 2: Values of the J_i magnetic exchange interactions computed for the *d1-d7* radical pairs of **1** found in the crystal structures obtained at 10K and 163K.

Dimer, *di*	10K		163K	
	d(Cu···Cu) / Å	J_i (cm^{-1})	d(Cu···Cu) / Å	J_i (cm^{-1})
d1	6.898	−10.2	6.916	−9.0
d2	6.876	−7.3	6.920	−8.7
d3	9.711	−0.3	9.781	<|0.05|
d4	9.769	−0.3	9.786	−0.13
d5	7.933	<|0.05|	8.104	<|0.05|
d6	8.443	<|0.05|	8.570	<|0.05|
d7	8.955	<|0.05|	9.009	<|0.05|

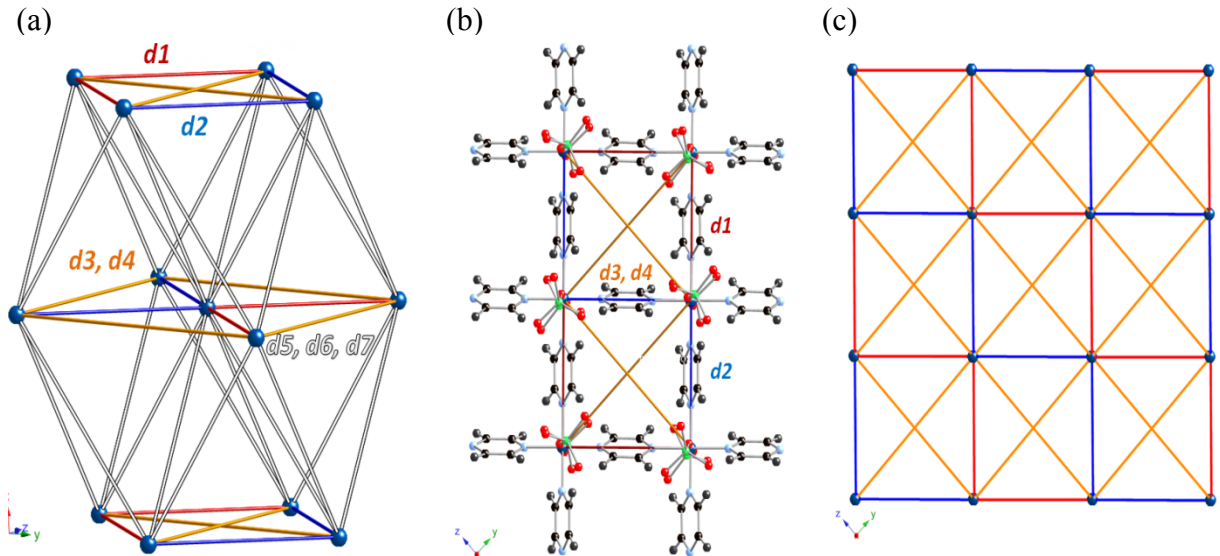*Figure 2:* (a) Schematic representation of all possible non-symmetry related radical-pairs d1-d7 in **1**. Note that d1-d4 give rise to *bc*-planes, which stack along the third direction (*a*-axis). Only copper atoms are shown. (b) Overlap of crystal structure and representation of non-negligible *J*(d1)−*J*(d4), which correspond to the magnetic building block. (c) 2D magnetic model of **1**. Blue dots represent Cu atoms of **1**. *J*(d1), J(d2) and J(d3)&*J*(d4) magnetic exchange interactions are represented as red, blue and orange lines, respectively.

The same analysis was also performed using the 163K crystal structure and the results showed only minor changes compared to the 10K analyzed data: the magnetic topology is preserved and so is the nature of the magnetic interactions within the crystal. However, as shown in Table 2, the effect of the thermal expansion is clear: the Cu⋯Cu distance increases for each radical-pair as the temperature increases and the corresponding J_{AB} value is thus affected. At 163K, dimers *d1* and *d2* have similar J_{AB} values (−9.0 vs. −8.7 cm^{-1}) in contrast with their analogues at 10K (−10.2 vs. −7.3 cm^{-1}). This is an example of how the anisotropic contraction of a crystal can affect the magnetic interactions between spin-carrier units in a different way, enhancing or reducing its AFM character. Note that at 163K the decrease of the J_3 and J_4 diagonal terms (see Figure 2b) reduces the competing interactions towards the magnetically dominant J_1 and J_2 interactions, which define a quasi-isotropic 2D magnetic topology. It follows that these two similar J_{AB} values (−9.0 vs. −8.7 cm^{-1}) may explain why a square lattice model was fairly successful in experimentally modeling the magnetic susceptibility data of **1**.[2d]

It should also be pointed out that the elongation of the Jahn-Teller axis (*a*-axis) from 13.825Å at 10K to 14.072Å at 163K does not imply changes in the magnetic topology of [Cu(pz)$_2$](ClO$_4$)$_2$, since it consists of magnetic *bc*-layers which do not interact along the *a*-axis (irrespective of the temperature at which the crystal has been crystallographically characterized). Besides, in **1**, pairs d1 and d2 are excellent examples (see Figure 4) of how unfeasible is to intend to relate the geometrical disposition of the radicals within the crystal and the magnitude of the J_{AB} magnetic interactions. Our study reveals that the electronic structure changes that are not observed by simple inspection must be taken into account and that each system must be approached in a different way. It thus follows that the symmetry of the whole radical and its arrangement with radical neighboring molecules play a fundamental role in the coupling of such complexes. However, the nature of the magnetic interaction cannot always be predicted a priori since subtle contributions arise from the radicals taken as a whole, their counterions, and bridging ligands, not just from the 'formal' spin-carrying moieties.

Using the J_{AB} values calculated in the previous step and after analysis of the resulting magnetic topology for the 10K and 163K crystal structures, a magnetic model of 16 radical centers in the 2D plane (2D16s) (Figure 2c) was chosen to reproduce the experimental magnetic susceptibility χ(T) and heat capacity C$_p$(T) data, within a regionally reduced density
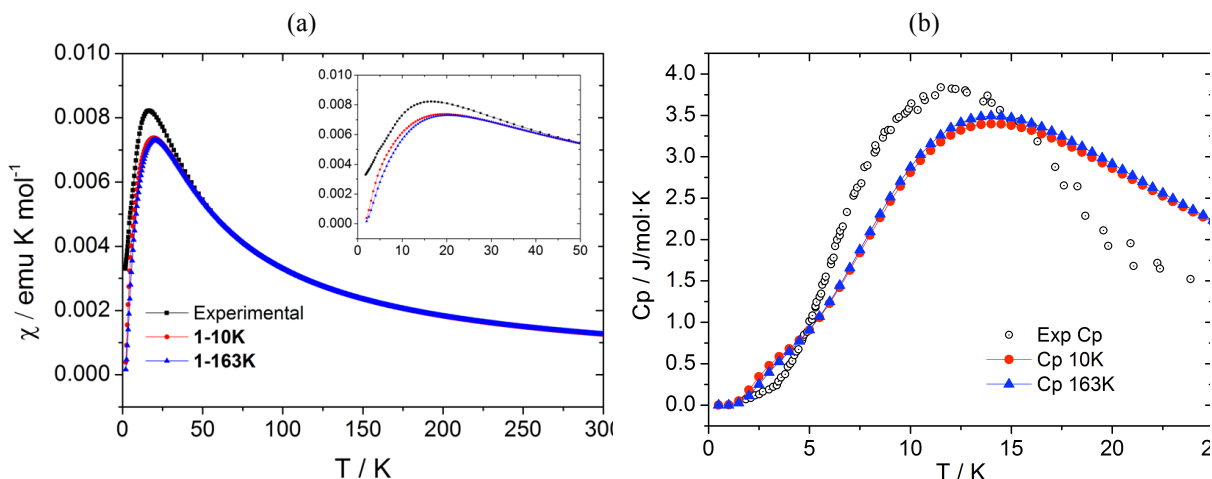
Figure 3: Comparison between (a) experimental (black line) and computed (red and blue lines) parallel χ(T) curves and (b) experimental (black symbols) and computed (red and blue lines) C_p(T) data using the 2D16s magnetic model (pictured in Figure 2c) at 10 and 163 K, respectively. See also in (a) an inset for the low temperature region of the χ(T) curve.

approach.[5] The simulated χ(T) curves show its maximum at 19.5K with a value of 0.0074 emu·mol^{-1}. Meanwhile, the maximum in the experimental curve is located at 16.5K and 0.0082 emu·mol^{-1}. Thus, the agreement between simulated and experimental data is remarkable, considering that, alternatively to other methodologies, the J_{AB} values are not fitted pursuing a perfect agreement with the experimental data. Besides, comparison between calculated and experimental χ(T) data indicates that, for the case of **1**, the simulation of χ(T) using the crystal structure obtained at 10K does not offer notable improvement with respect to the χ(T) data computed using the crystal structure at 163K (see Figure 3a). Therefore, the magnetic χ(T) response is not significantly dependent upon the thermal lattice expansion of the crystal structure as temperature changes, even though the calculated exchange couplings vary slightly from 10 K to 163K. Let us clarify that the computed χ(T) curve of **1** behaves as the parallel component to the easy axis of χ(T) of a typical single crystal AFM with an abrupt decay towards zero as temperature decreases, which it is now compared to the experimental χ$_∥$(T) data obtained from single crystal sample.

Regarding heat capacity, we will focus on the low temperature region since it will be most sensitive to magnetic dimensionality changes (see Figure 3b and Supporting Information S5). The calculated C_p(T) data using the **1-10K** magnetic model initially rise more slowly than experiment at low temperature, as suggested in the literature.[11] It then reaches its maximum

value at a slightly higher temperature: 14K in our simulations against an experimental 11.5K value. Muon spin-relaxation (μ-SR$^+$) measurements have revealed that **1** undergoes a transition from a 2D AFM to a 3D ordered state at 4.21 K. The simulation of $C_p(T)$ shows an anomaly ranging from 2.0 to 4.5 K, i.e., around the Néel temperature of 4.21 K. Our results also show that the calculated $C_p(T)$ data in the low temperature region (0-10K) does not depend on the magnetic field and, thus, this anomaly is not an artifact of it (see Supporting Information S5). In order to confirm whether this anomaly could be seen as a signature of long-range order, crystallographic data below the transition temperature would be required to test if the magnetic topology becomes a set of 3D AFM layers with finite interlayer couplings (i.e. with *d5-d7* radical pairs showing significant J_{AB} values).

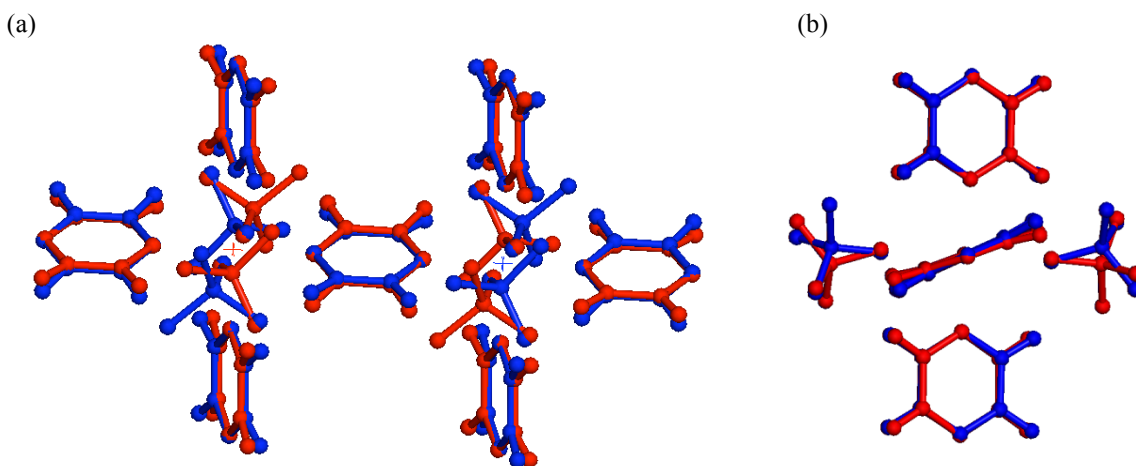(a)   (b)

Figure 4. Overlap of (a) lateral and (b) top views of radical pairs d1 (red) and d2 (blue) of **1**.

2. The role of pyrazine ligands and ClO_4^- counterions in J_{AB} dominant magnetic interactions

Now that the J_{AB} values have successfully reproduced the experimental $\chi(T)$ and $C_p(T)$ curves, we turn our attention to rationalizing the strength of the dominant magnetic couplings (J_1 and J_2). For years, research has been oriented to understand how the magnetic exchange through pyrazine can vary considerably –from roughly 0 to 15 K.[25] Very interestingly, [Cu(pz)$_2$](ClO$_4$)$_2$ **1** is an example of significantly different J_{AB}'s within the same compound. Note that J_1 and J_2 correspond to through-bond interactions mediated by pyrazine rings (Figure 2a), whose value is notably different (25%) despite presenting an almost identical radical pair arrangement (see Figure 4). In the following, we address the numerical difference between J_1 and J_2 by evaluating the role of the copper−pyrazine skeleton (i.e. framework) and

the role of the perchlorate counterions. Henceforth, for the sake of clarity, the discussion will just concern the results for the 10K-crystal structure, hereafter **1**.

2.1 Pyrazine pz ligands

First, calculations of J_{AB} values using d_1 and d_2 radical pairs were performed without the perchlorate counterions to evaluate the contribution of the pyrazine−copper skeleton to the magnetism of $[Cu(pz)_2](ClO_4)_2$ (for these sets of calculations, we consider the radicals as $[Cu(pz)_2]^{2+}$ units). The absence of the counterion affects the J_{AB} values symmetrically: J_1 decreases its antiferromagnetic character from −10.2 cm^{-1} to −4.9 cm^{-1} while J_2 diminishes from −7.3 cm^{-1} to −4.0 cm^{-1}. It thus follows that the effect that can be attributed to the non-symmetric nature of the Cu−pz frame contributes ±0.9 cm^{-1} to the exchange J_{AB} couplings for this compound. The question now is to clarify this issue.

In a first attempt to understand this effect, we performed J_{AB} calculations as a function of the dihedral angle pictured in Figure 5a (see (pz)N···Cu···N-C(pz) in light yellow). From this set of calculations we concluded that, in the absence of counterions, the canting of the central pyrazine is not the origin of the different J_{AB} values for *d1* and *d2* (see Supporting Information S6). Instead, the influence of the *shearing*-like distorsion of the central pyrazine ring must be studied since both Cu···Cu distances as well as Cu···N(pz) and (pz)N···N(pz) distances are slightly different in *d1* and *d2* (see Cu(orange)···Cu(orange), Cu(orange)··N(pz, blue) and (pz, blue)N···N(pz, blue) in Figure 5b).

In order to quantify the relative change estimations in the pz ring, we will resort to the bond length alternation BLA parameter,[26] which is widely used in non-linear optical materials. As for the pz ring, BLA will be defined as $\Delta R = r_1 - (r_2 + r_3)/2$.[27] Table 3 shows these geometrical parameters for *d1* and *d2* and also how a slight variation of the distance (*d1'*) affects the associated J_{AB} value. Large ΔR suggests larger shearing-like distortions of the pz ring. It thus follows that the pz ring in *d1* is more asymetrically distorted than in *d2*. Accordingly, in (Cu-pz)-based magnets it appears that large shearing-like distortions are connected to larger AFM character. These calculations indicate that, in the absence of counterions, the very slight differences in the inter-atomic distances present in the Cu-N···N-Cu magnetic pathway (see Figure 5b) are responsible for the different value of *d1* and *d2* magnetic interactions in **1**, irrespective of the canting of this central pyrazine.
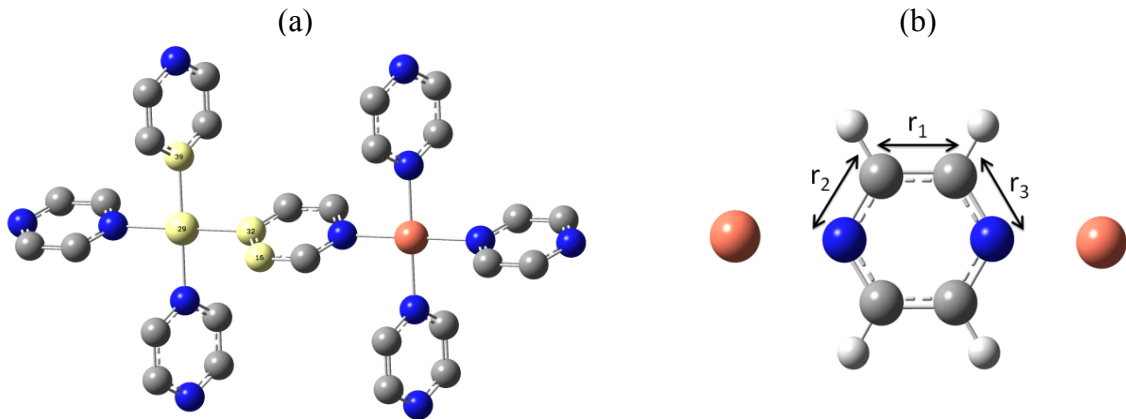
Figure 5. (a) Dihedral angle (pz)N⋯Cu⋯N-C(pz) (highlighted in light yellow) chosen to measure the role of the canting of the central pyrazine ring to the Cu−pz frame contribution. (b) Schematic view of the Cu−pz−Cu magnetic pathway. The study of the distorsion of the central pyrazine ring includes distances between (orange)Cu⋯Cu(orange), (orange)Cu⋯N(pz, blue) and (pz, blue)N⋯N(pz, blue). For discussion purposes, the BLA parameter is defined as: $\Delta R = r_1 - (r_2 + r_3)/2$. Hydrogen atoms have been removed for clarity and perchlorate counterions are not included in this set of calculations. Color code: C (gray), N (blue), Cu (orange).

Table 3: Values of the J_{AB} magnetic exchange interactions computed for the *d1* and *d2* radical pairs of **1** found in the 10K crystal, and for the same radical pairs upon variation on the Cu⋯N(pz) and the (pz)N⋯N(pz) distances. All distances in Å and J_{AB} values in cm^{-1}. *ΔR* measures the bond-length alternation in the pyrazine ring as $[r_1 - (r_2 + r_3)/2]$ Å.

	d(Cu⋯Cu)	d(Cu⋯N(pz))	d(N(pz)⋯N(pz))	J_{AB}	*ΔR* /Å
d1	6.898	2.061	2.778	**−4.9**	0.046
d1'	6.898	2.074	2.750	−4.5	0.044
d2	6.876	2.060	2.757	**−4.0**	0.037

Table 4: Values of the J_{AB} magnetic exchange interactions computed for the *d1* and *d2* radical pairs of **1** found in the 10K crystal, and for the same radicals pairs but once the ClO$_4^-$ counterions have been exchanged.

Name	Cu-pz-Cu	Counterion	J_{AB} / cm^{-1}
d1(d1)	*d1*	*d1*	−10.23
d1(d2)	*d1*	*d2*	−7.64
d2(d1)	*d2*	*d1*	−9.85
d2(d2)	*d2*	*d2*	−7.33

(a)   (b)
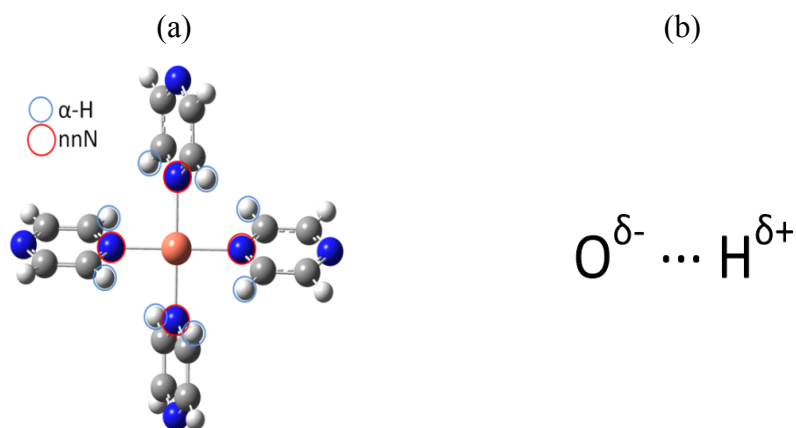
Figure 6: (a) Representation of the alpha-hydrogen atoms (α−H, highlighted in blue) and nearest-neighboring nitrogen atoms (nnN, highlighted in red). (b) Scheme to picture the relation between the strength of a hydrogen bond and the charge polarization of the atoms involved.

2.2 Counterions

Secondly, the impact of the orientation of the ClO_4^- counterions was evaluated by computing J_{AB} for *d1* with counterions placed as in *d2* and *vice versa*. According to Table 4, counterions in the *d1* orientation enhance the AFM character of the radical···radical coupling resulting in J_{AB}'s of about −10 cm^{-1}, while for counterions in *d2* the AFM exchange strength is diminished by *ca.* 2.5 cm^{-1} (compare |*d1(d1)*−*d1(d2)*| against |*d2(d2)*−*d2(d1)*| in Table 4). At this point, our hypothesis was that this difference in the strength of the magnetic exchange could be due to the presence of hydrogen bonds. From a computational point of view, let us mention here that Ruiz and coworkers had already raised the question on exchange coupling of transition-metal ions through hydrogen bonding.[28] After an analysis of the MSK charges[19] of the first-sphere of the α−hydrogen atoms around the Cu···counterion moiety (see Figure 6a) for *d1* and *d2*, one realizes that the α−H sphere using *d2* counterions has more charge (1.96 a.u.) than using *d1* (1.79 a.u.). This fact could be taken as a signature for a larger degree of hydrogen bonding in *d2*, which is empirically known to enhance FM interactions.[29] Note that the hydrogen bonding qualitative argument is based on the fact that it is assumed that the more polarized the hydrogen atoms are, the stronger the bond is (see Figure 6b). It follows that a less AFM J_{AB} value should be thus expected for radical pairs with a larger contribution from hydrogen bonding (*J2* vs. *J1*). The presence of hydrogen bonding in crystals of **1** had already been confirmed by Choi *et al.*,[30] who suggested that such hydrogen bonding might influence the structure and magnetism of this entire family of low-dimensional quantum antiferromagnets.
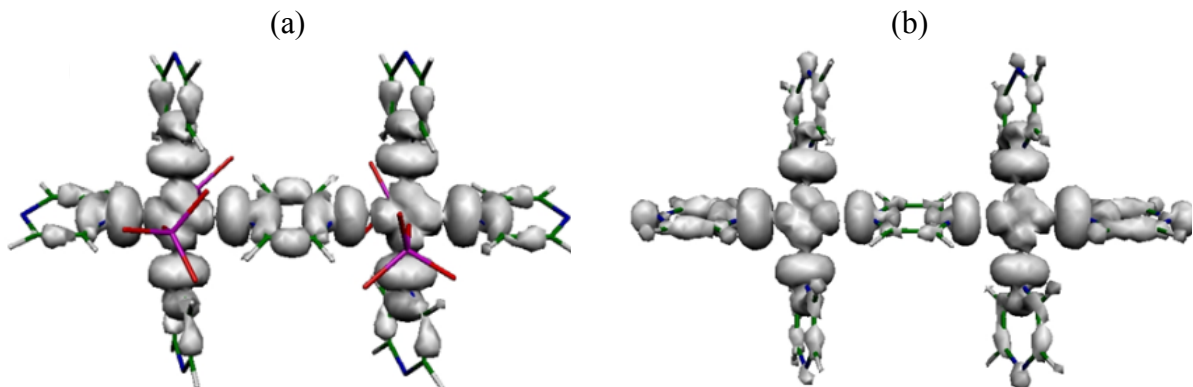
Figure 7: (a) Representation of the triplet spin density for *d1* radical pair of **1** and (b) its analogue without ClO_4^- counterions. Notice the different spin density carried by the central pyrazine ring. In both representations the isosurface is 0.0005 a.u.

A further exploration of the effect of the counterions offers valuable insight into how the magnetic coupling could be tuned. For instance, the presence of counterions is manifested by an increase in the spin density between the Cu(II) ions, along the Cu···N(pz)N···Cu axis (see Figure 7) and, as a result, the magnetic interaction is enhanced. The presence of hydrogen bonding between the O atoms of the perchlorate ions and H atoms of the pyrazine rings may be partly responsible for this effect, although no clear magneto-structural correlation has been yet found.

2.3. Hydrogen bonding

The next question to put forward is: what will happen if one tunes the strength of the hydrogen bonds? The role of the counterions is further analyzed by replacing the perchlorate ions of the original crystal structure by a family of counterions with the same tetrahedral symmetry (namely BF_4^-, BCl_4^- and BBr_4^-), and computing the corresponding J_{AB} values (see Table 5). In all calculations, the experimental crystal structure frame of *d1* and *d2* pairs of radicals has been preserved in order to avoid the effect of a geometry distortion on the J_{AB} values if an optimization procedure was performed. Although we describe these new counterions (BF_4^-, BCl_4^- and BBr_4^-) with the crystal geometry of the original ClO_4^-, the effect of their un-optimized structure is approximately cancelled out when obtaining J_{AB} as the difference of spin states. Let us stress that these calculations do not intend to predict the exact value of the magnetic exchange coupling (J_{AB}) for the corresponding hypothetical structures, but to provide an educated tendency as a function of the electronegativity (EN) of the external

Table 5: Values of the J_{AB} magnetic exchange interactions computed for the *d1* and *d2* radical pairs of **1** found in the 10K crystal once ClO_4^- have been replaced by counterions with tetrahedral symmetry, namely, BF_4^-, BCl_4^- and BBr_4^-. The electronegativity EN of the external atoms of the counterion and the average spin population on the N atoms of the central pyrazine is also shown.

Counterion	J_1 /cm^{-1}	J_2 /cm^{-1}	EN	(N-pyz)
No Counterion	−4.9	−4.0		0.0643
ClO_4^-	−10.2	−7.3	3.44 (O)	0.0829
BF_4^-	−10.1	−7.1	3.98 (F)	0.0825
BCl_4^-	−12.4	−9.3	3.16 (Cl)	0.0881
BBr_4^-	−12.9	−11.0	2.96 (Br)	0.0905

atoms of the counterion.[31] According to the results shown in Table 5, together with the effect pictured in Figure 7a, one can conclude that for this system the spin density on the central pyrazine (and, as a consequence, the magnetic interaction J_i) increases when counterions with less EN external atoms such as bromide or chloride are used. In accordance, counterions with highly EN external atoms such as fluoride or oxygen are able to drain more electron density from the central pyrazine, and, in turn, reduce the magnetic exchange coupling. Let us stress the fact that for the whole set of counterions that we have studied, the difference between J_1 and J_2 is always about *ca.* 25%, reinforcing the previous analysis on the role of the counterion orientation. Furthermore, in the absence of counterions (Figure 7b), the central pyrazine drops its spin density and, in turn, the AFM character of the corresponding exchange coupling decreases.

In a last attempt to relate the spin density of the central pyrazine with the presence of hydrogen bonding, we have evaluated the charge distribution[19] of the Cu ions and their environment. For clarity, Table 6 shows only the results using the dimer 1 *(d1)* radical pair arrangement, which is taken as the reference. Again, there is a clear relationship between the EN of the external atoms of the counterion and the charge distribution. As the EN decreases for the set of calculations with BX_4^- (X = F, Cl, Br), the counterion remains more positively charged as its electron density is transferred to the Cu atoms. This results in a larger charge and more electron density carried by Cu and nearest neighbor N atoms (|Cu-nnN| in Table 6) as the EN decreases, which is consistent with the picture of the largest atom contribution to the $[Cu(pz)_2](ClO_4)_2$ radical SOMO (Figure 1b). It thus follows that the $[Cu(pz)_2](BBr_4)_2$ radicals can couple better, as the larger J_{AB} indicates.

Table 6: MSK atomic charges of *d1* radical pair for the counterions (CI), the copper atom (Cu) and the polarization of the atoms involved in the SOMO (Cu and nearest neighboring nitrogen atoms, |Cu-nnN|) relative to the value computed using perchlorate ligands. Electronegativity (EN) value for external atoms of the counterions and J_{AB} (in cm^{-1}) values are also given.

Counterion	J_l/cm^{-1}	EN	CI	Cu	|Cu-nnN|
ClO_4^-	−10.2	3.44 (O)	-	-	-
BF_4^-	−10.1	3.98 (F)	0.0	-0.1	0.1
BCl_4^-	−12.4	3.16 (Cl)	0.1	-0.3	0.3
BBr_4^-	−12.9	2.96 (Br)	0.2	-0.3	0.2

Let us now recapitulate the main ideas featured in this section. For **1**, we have quantified the effect of the copper−pyrazine skeleton in the absence of counterion to be roughly 0.9 cm^{-1}, and the effect of the counterion orientation to be 2.5 cm^{-1}. Interestingly, the difference on the value of the J_{AB} magnetic coupling for pairs *d1(d1)* and *d2(d2)* (see Table 4) is 2.9 cm^{-1} instead of 3.4 cm^{-1} (resulting from the sum of the two effects previously analyzed: 0.9 and 2.5 cm^{-1}). This numerical discrepancy indicates a cooperation between both effects (skeleton and counterions) when the pair of radicals is fully considered. Once the presence of hydrogen bonding has been anticipated, one can argue that the origin of this cooperation is the inclusion of a different amount of hydrogen bonding in the two conformations (*d1 / d2*) of the skeleton frame that cannot be detected when the counterion is absent. Similarly, one can think of the energy of the H_2 molecule to be the sum of the energy of the first H atom, the energy of the second H atom, and also the energy arising from the interaction between them. This is in clear contrast with the study performed on bis(2,3-dimethylpyrazine)dihalocopper(II) complexes, $Cu(2,3-dmpz)_2Cl_2$ and $Cu(2,3-dmpz)_2Br_2$,[8] where the strength of the J_{AB} magnetic coupling between radicals was arithmetically calculated by dissecting all magnetic components coming from skeleton and substituents since there were no counterions that could contribute with hydrogen bonding.

This kind of analysis can be alternatively performed in the framework of wavefunction methodologies by adding/subtracting the proper orbitals in the variational (DDCI) or perturbative (CASPT2) treatment after the selection of the best active space. This strategy has been successfully carried out in the past for similar organometallic systems.[32] However, this level of calculation is absolutely unaffordable to study $[Cu(pz)_2](ClO_4)_2$ since it would require an excessively large active space.[33] Furthermore, the results obtained by the use of different counterions in order to study the role of weak interactions in $[Cu(pz)_2](ClO_4)_2$ are far more

intuitive and easy to understand for the experimental community than other more algebraic approaches.

[Cu(pz)$_2$](ClO$_4$)$_2$, **1**, can thus be regarded as an excellent example of how different effects sum up to reveal a 2D macroscopic magnetic behavior. For instance, we have learned that the 2D copper−pyrazine skeleton is not as rigid a packing unit as one could think of upon initial examination. The internal structure of the pyrazine could thus result in different values of magnetic coupling J_{AB} for the same given radical···radical magnetic interaction. The orientation of the ClO$_4^-$ counterions −although being closed-shell species− has proven to be crucial when evaluating the magnetic coupling strength J_{AB}. The electronegativity EN of the counterions is another key factor since low EN favors a better radical···radical coupling, and in turn AFM J_{AB} is larger. In addition, hydrogen bonds have been numerically found to be enhancers of ferromagnetic interactions (in agreement with experimental literature[29]). Finally, **1** is an example of how the anisotropic thermal contraction of a crystal can affect the magnetic interaction between radicals either enhancing or reducing its AFM character. Therefore, the First-Principles Bottom-Up study of [Cu(pz)$_2$](ClO$_4$)$_2$ teaches us about how to design tailored copper−pyrazine based magnets; namely, by controlling: (i) the internal structure of the Cu−pz skeleton, (ii) the spin distribution on the pyrazine rings which is driven by the electronegativity of the counterions, (iii) the presence of hydrogen bonds between pyrazine and counterions, and (iv) the temperature at which the experiment is conducted.

CONCLUSIONS

A First-Principles Bottom-Up study of the magnetic properties of [Cu(pz)$_2$](ClO$_4$)$_2$ unravels its 2D magnetic topology due to two antiferromagnetic J_1 and J_2 interactions through bridging pyrazine ligands. Although presenting a very similar molecular arrangement, the numerical value of the two magnetically significant J_{AB} couplings differ by 25% (−10.2 vs. −7.3 cm^{-1}). The agreement between simulated and experimental χ(T) data is remarkable in the whole range of temperatures; in fact, we are even able to reproduce the temperature at which the maximum value of χ is reached. This is a fingerprint of molecule-based materials whose magnetic response is not significantly dependent upon anisotropic thermal contraction of the crystal structure as temperature changes, even though the calculated exchange couplings slightly vary from 163 K to 10K. Let us remark that the quasi-isotropic 2D magnetic topology

at 163 K may explain why a square lattice model was fairly successful in experimentally modeling the magnetic data of $[Cu(pz)_2](ClO_4)_2$. The available experimental $C_p(T)$ data (0−25K) is also well reproduced with our results: in our simulations, it reaches its maximum value at 14K against the experimental 11.5K temperature. Interestingly, the simulated $C_p(T)$ values show an anomaly close to the Néel temperature of 4.21 K, which has been determined by μ-SR[+] experiments and associated with a transition from a 2D AFM to a 3D ordered state.

The canting of the central pyrazine ring appears not to be the origin of the different J_{AB} values for *d1* and *d2*, but rather the *shearing*-like distorsion of the pyrazine rings. The role of the ClO_4^- counterions is believed to be to increase the spin density along the magnetic pathway that links the Cu(II) ions through a pyrazine ring, thus increasing the magnetic interaction. Studies performed using a series of counterions with different electronegativity (EN) show that the spin density on the central pyrazine increases when low EN external ions such as bromide or chloride are used as counterions, while highly EN external ions such as fluoride or oxygen are able to drain more electron density from the Cu atoms, and in turn, reduce the magnetic exchange coupling. Finally, the authors have considered the presence of hydrogen bonding between the O atoms of the perchlorate ions and H atoms of the pyrazine rings. In $[Cu(pz)_2](ClO_4)_2$, the hydrogen bonds have been numerically found to be enhancers of FM interactions, since their role consists in diminishing the AFM character of the J_{AB} interactions.

We can conclude that the $|3\ cm^{-1}|$ numerical difference between computed exchange J_1 and J_2 couplings is due to the effect of the *shearing*-like distorsion of the pyrazine rings, the orientation of the ClO_4^- counterions and a hitherto skeleton-counterion cooperation arising from different hydrogen bonding contribution in *d1*/*d2*, which contribute +0.9 cm^{-1} (31.0%), +2.5 cm^{-1} (86.2%) and -0.5 cm^{-1} (-17.2%), respectively –in effect showing how to "divide the spoils" between the various contributions to the overall exchange.

Supporting Information

S1. Spin density and SOMO of $[Cu(pz)_2](ClO_4)_2$ radical − S2. Basis set − S3. Magnetic susceptibility from powder / single crystal samples − S4. View of d1-d7 radical pairs − S5. Heat capacity − S6. Canting of central pyrazine ring − S7. GAUSSIAN09 reference

References

[1] (a) Awwadi, F.F.; Landee, C.P.; Turnbull, M.M.; Twamley, B.; Wells, B.M. *Polyhedron* **2005**, *24*, 2153. (b) Wang L., Sun, X.P.; Liu, M.L.; Gao, Y.Q.; Gu, W.; Liu X. *J. Cluster Sci.* **2008**, *19*, 531. (c) Handa, M.; Ishitobi, Y.; Yakuwa, T.; Yoshioka, D.; Ishida, H.; Mikuriya, M.; Hiromitsu, I.; Tanaka, H.; Ikeue T. *Bull. Chem. Soc. Jpn.* **2009**, *82*, 1277. (d) Ren, Y.P.; Kong, X.J.; Hu, X.Y.; Sun, M.; Long, L.S.; Huang, R.B.; Zheng, L.S. *Inorg. Chem.* **2006**, *45*, 4016.

[2] (a) Guo, H.X.; Weng, W.; Li, X.Z.; Liang, M.; Zheng, C.Q.; *Acta Crystallogr., Sect. C: Cryst. Struct. Commun.* **2008**, *64*, m314. (b) Selmani, V.; Landee, C.P.; Turnbull, M.M.; Wikaira, J.L.; Xiao, F. *Inorg. Chem. Commun.* **2010**, *13*, 1399. (c) Halasyamani, P.; Heier, K.R.; Willis, M.J.; Stern, C.L.; Poeppelmeier, K.R.; *Z. Anorg. Allg. Chem.* **1996**, *622*, 479. (d) Woodward, F.M.; Gibson, P.J.; Jameson, G.; Landee, C.P.; Turnbull, M.M; Willett, R.D., *Inorg. Chem.* **2007**, *46*, 4256-66.

[3] (a) de Jongh, L.J. *Magnetic Properties of Layered Transition Metal Compounds*, Kluwer Academic, Hingham, MA, **1989**. (b) Kim, J.; Troyer, M. *Phys. Rev. Lett.* **1998**, *80*, 2705. (c) Rushbrooke, G.S.; Baker, G.A. and Wood, P.J. *Phase Transitions and Critical Phenomena,* Academic, New York, **1974**. (d) Woodward, F.M.; Albrecht, A.S.; Wynn, C.M.; Landee, C.P.; Turnbull, M.M. *Phys. Rev. B.* **2002**, *65*, 144412. (e) Keith, B.C.; Landee, C.P.; Valleau, T.; Turnbull, M.M.; Harrison, N. *Phys. Rev. B.* **2011**, *84,* 104442.

[4] (a) Calzado, C.J. *Chem. Eur. J.* **2013**, *19*, 1254. (b) Xiang, H.; Lee, C.; Koo, H.-J.; Gonga, X.; Whangbo, M.H. *Dalton Trans.* **2013**, *42*, 823. (c) Yamaguchi, H.; Nagata, S.; Tada, M.; Iwase, K.; Ono, T.; Nishihara, S.; Hosokoshi, Y.; Shimokawa, T.; Nakano, H.; Nojiri, H.; Matsuo, A.; Kindo, K.; Kawakami, T. *Phys. Rev. B* **2013**, *87*, 125120. (d) Palii, A.; Tsukerblat, B.; Clemente-Juan, J.M.; Coronado, E. *Int. Rev. Phys. Chem.* **2010**, *29*, 135. (e) Igor Negodaev,I.; de Graaf, C.; Caballol, R. *J. Phys. Chem. A* **2010**, *114*, 7553. (f) Sasmal, S.; Hazra, S.; Kundu, P.; Majumder, S.; Aliaga-Alcalde, N.; Ruiz, E.; Mohanta, S. *Inorg. Chem.* **2010**, *49*, 9517. (g) Fliegl, H.; Fink, K.; Klopper, W.; Anson, C.E.; Powell, A.K.; Clérac, R. *Phys. Chem. Chem. Phys.* **2009**, *11*, 3900. (h) Hairie, T. Robert, V. Petit, S. *Phys. Rev. B* **2006**, *74*, 052408. (i) Moreira, I.P.R.; Illas, F. *Phys. Chem. Chem. Phys.* **2006**, *8*, 1645. (j) Borrás-Almenar, J.J.; Clemente-Juan, J.M.; Coronado, E.; Tsukerblat, B.S. *J. Comp. Chem.* **2001**, *22*, 985. (k) Kortus, J.; Hellberg, C.S.; Pederson, M.R. *Phys. Rev. Lett.* **2001**, *86*, 3400.

[5] (a) Deumal, M.; Bearpark, M.J.; Novoa, J.J.; Robb, M.A. *J. Phys. Chem. A* **2002**, *106*, 1299. (b) Vela, S.; Deumal, M.; Turnbull, M.M.; Novoa, J.J. *Theor. Chem. Acc.* **2013**, *132*, 1331

6   (a) Deumal, M.; Giorgi, G.; Robb, M.A.; Turnbull, M.M.; Landee, C.P.; Novoa, J.J. *Eur. J. Inorg. Chem.* **2005**, 4697–4706. (b) Shapiro, A.; Landee, C.P.; Turnbull, M.M.; Jornet, J.; Deumal, M.; Novoa, J.J.; Robb, M.A.; Lewis, W. *J. Am. Chem. Soc.* **2007**, *129*, 952-959 (c) Li, L.; Turnbull, M.M.; Landee, C.P.; Jornet, J.; Deumal, M.; Novoa, J.J.; Wikaira, J.L. *Inorg. Chem.* **2007**, *46*, 11254−11265. (d) Jornet-Somoza, J.; Deumal, M.; Landee, C. P.; Turnbull, M. M.; Novoa, J. J. *Inorg. Chem.* **2010**, *49*, 8017-8024.

7   Jornet-Somoza, J.; Deumal, M.; Robb, M.A.; Landee, C.P.; Turnbull, M.M.; Feyerherm, R.; Novoa, J.J. *Inorg. Chem.* **2010**, *49*, 1750-1760.

8   Jornet-Somoza, J.; Codina-Castillo, N.; Deumal, M.; Mota, F.; Novoa, J.J.; Butcher, R.T.; Turnbull, M.M.; Keith, B.; Landee, C.P.; Wikaira, J.L. *Inorg. Chem.* **2012**, *51*, 6315-6325.

9   (a) Novoa, J.J.; Deumal, M.; Jornet-Somoza, J. *Chem. Soc. Rev.* **2011**, *40*, 3182. (b) Clarke, C.S.; Jornet-Somoza, J.; Mota, F.; Novoa, J.J.; Deumal, M. *J. Am. Chem. Soc.* **2010**, *132*, 17817. (c) Vela, S.; Deumal, M.; Ribas-Arino, J.; Novoa, J.J. *Inorg. Chem.* **2012**, *51*, 8646-8648.

10   Xiao, F.; Woodward, F.M.; Landee, C.P.; Turnbull, M.M.; Mielke, C.; Harrison, N.; Lancaster, T.; Blundell, S.J.; Baker, P.J.; Babkevich, P.; Pratt, F.L. *Phys. Rev. B* **2009**, *79*, 134412.

11   Lancaster, T.; Blundell, S.J.; Brooks, M.L.; Baker, P.J.; Pratt, F.L.; Manson, J.L.; Conner, M.M.; Xiao, F.; Landee, C.P.; Chaves, F.A.; Soriano, S.; Novak, M.A.; Papageorgiou, T.P.; Bianchi, A.D.; Herrmannsdörfer, T.; Wosnitza, J.; Schlueter, J.A. *Phys. Rev. B* **2007**, *75*, 094421.

12   Darriet, J.; Haddad, M. S.; Duesler, E. N.; Hendrickson, D. N. *Inorg. Chem.* **1979**, *18*, 2679

13   Roisnel, T.; Rodríguez-Carvajal, J.; Materials Science Forum, Proceedings of the Seventh European Powder Diffraction Conference (EPDIC 7), **2000**, pp.118-123, Ed. Delhez, R. and Mittenmeijer, E.J.

14   (a) Noodleman, L. *J. Chem. Phys.* **1981**, *74*, 5737. (b) Noodleman, L.; Davidson, E.R. *Chem. Phys.* **1986**, *109*, 131.

15   From the General Heisenberg Hamiltonian $\hat{H} = -2\sum_{A,B}^{N} J_{AB}\hat{S}_A \cdot \hat{S}_B$, for a pair of A and B radicals, the J_{AB} value is computed as the energy difference between biradical open-shell singlet S and triplet T states, $\Delta E^{S-T} = E^S - E^T = 2J_{AB}$. The criteria chosen to compute the energy difference is $\Delta E^{S-T} = E^S - E^T = = 2(E_{BS}^S - E^T)/(1 + S_{ab})$. Open-shell singlet systems separate alpha spin density and beta spin density on different radicals. In our case, once the broken symmetry approximation is applied, the resulting overlap between the alpha SOMO and the beta SOMO is zero. Thus those orbitals are localized on each of the two radicals. This leads to $S_{ab} = 0$. As a conclusion $J_{AB} = E_{BS}^S - E^T$.

16   Parr, E.G.; Yang, W. *Density Functional Theory of Atoms and Molecules*, Oxford University Press, New York, **1989**.

17   (a) Becke, A.D. *Phys. Rev. A* **1988**, *38*, 3098; (b) Becke, A.D. *J. Chem. Phys.* **1993**, *98*, 5648; (c) Lee, C.; Yang, W.; Parr, R.G. *Phys. Rev. B* **1988**, *37*, 785.

18   Schaefer, A.; Huber, C.; Ahlrichs, R. *J. Chem. Phys.*, **1994**, *100*, 5829.

19   (a) Singh, U.C.; Kollman, P.A. *J. Comp. Chem.*, **1984, *5*, 129. (b) Besler B.H.; Merz Jr., K.M.; Kollman, P.A. *J. Comp. Chem.*, **1990**, *11*, 431.

20   Gaussian 09, Revision B.01, Frisch, M.J. et al., Gaussian, Inc., Wallingford CT, **2009**.

[21] (a) Deumal, M.; Bearpark, M.J.; Robb, M.A.; Pontillon, Y.; Novoa, J.J. *Chem. Eur. J.* **2004**, *10*, 6422. (b) Jornet-Somoza, J.; Deumal, M.; Turnbull, M.M.; Novoa, J.J. *Polyhedron*, **2009**, *28*, 1965.

[22] Reference to statistical mechanics expression of magnetic properties: Carlin, R.L. *Magnetochemistry*; Springer-Verlag: Berlin, **1986**

[23] Malrieu, J.-P.; Guihéry, N. *Phys. Rev. B* **2001**, *63*, 085110

[24] In practice, J_{AB} interactions whose absolute value is larger than 0.05 cm^{-1}.

[25] (a) Hong, D.-M.; Wei, H.-H.; Chang, K.-H.; Lee, G.-H.; Wang, Y.T.-C., *Polyhedron* **1998**, *17*, 3565-3573. (b) Haynes, J.S.; Sams, J.R.; Thompson, R.C. Can. J. Chem. **1988**, *66*, 2079-87. (c) Richardson, H.W.; Wasson, J.R.; Hatfield, W.E. Inorg. Chem. **1977**, *16*, 484-6. (d) Butcher, R.T.; Landee, C.P.; Turnbull, M.M.; Xiao, F. Inorg. Chim. Acta. **2008**, *361*, 3654-58. (e) Awwadi, F.F.; Dawe, L.N.; Landee, C.P.; Turnbull, M.M. *J. Coord. Chem.* **2012**, *65*, 3064-74. (f) Haynes, J.S.; Rettig, S.J.; Sams, J.R.; Thompson, R.C.; Trotter, J. Can. J. Chem. **1987**, *65*, 420-6.

[26] Gorman, C.B.; Marder, S.R. *Proc. Natl. Acad. Sci. USA* **1993**, *90*, 11297

[27] Murugan, N.A.; Kongsted, J.; Rinkevicius, Z.; Agren, H. *Proc. Natl. Acad. Sci. USA* **2010**, *107*, 16453

[28] Desplanches, C.; Ruiz, E.; Rodríguez-Fortea, A.; Alvarez, S. *J. Am. Chem. Soc.* **2002**, *124*, 5197.

[29] (a) Romero, F.M.; Ziessel, R.; Bonnet, M.; Pontillon, Y.; Ressouche, E.; Schweizer, J.; Delley, B.; Grand, A.; Paulsen, C. *J. Am. Chem. Soc.* **2000**, *122*, 1298. (b) Maspoch, D.; Catala, L.; Gerbier, P.; Ruiz-Molina, D.; Vidal-Gancedo, J.; Wurst, K.; Rovira, C.; Veciana, J. *Chem. Eur. J.* **2002**, *8*, 3635.

[30] Choi, J.; Woodward, J.D.; Musfeldt, J.L.; Landee, C.P.; Turnbull, M.M. *Chem. Mater.* **2003**, *15*, 2797

[31] They are hypothetical since the counterions do not occupy their equilibrium positions within the crystal. Note that the BF_4^- compound was published some years ago (see ref. 2d).

[32] Bandeira, N.A.G.; Maynau, D.; Robert, V.; Le Guennic, B. *Inorg. Chem.* **2013**. DOI: 10.1021/ic400517z

[33] For $[Cu(pz)_2](ClO_4)_2$ a possible choice of the CASSCF active space would consist of 70 electrons in 40 orbitals, namely, (i) 2 electrons on the 2 magnetic orbitals of the Cu atoms: (2,2); (ii) 2 electrons on the σ and σ* orbitals of each C(pz)-H bond of the central pz: (2,2)*4 = (8,8); and (iii) 6 electrons on the three lone pairs of each Oxygen atom of the perchlorate counterions, which are susceptible of forming hydrogen bonds. At least, 10 Oxygen atoms may be involved: (6,3)*10 O atoms = (60,30).

Graphical abstract

Table of Contents synopsis

A First-Principles Bottom-Up computational study of $[Cu(pz)_2](ClO_4)_2$ shows a remarkable agreement in the whole range of temperatures between simulated and experimental magnetic susceptibility and heat capacity data. The antiferromagnetic behavior of $[Cu(pz)_2](ClO_4)_2$ is due to a 2D antiferromagnetic topology. The role of pyrazine ligands, perchlorate counterions and hydrogen bonding is explored in order to interpret, and ultimately be able to tune, the J_{AB} exchange coupling interactions between radicals.

Table of Contents graphic